

Dispersion and the Speed-Limited Particle-in-Cell Algorithm

Thomas G. Jenkins,^{1, a)} Gregory R. Werner,² and John R. Cary^{1,2}

¹⁾ *Tech-X Corporation, 5621 Arapahoe Avenue Suite A, Boulder, Colorado 80303, USA*

²⁾ *Center for Integrated Plasma Studies, University of Colorado, Boulder, Colorado 80309, USA*

(Dated: 1 September 2021)

This paper discusses temporally continuous and discrete forms of the speed-limited particle-in-cell (SLPIC) method first treated by Werner *et al.* [Phys. Plasmas **25**, 123512 (2018)]. The dispersion relation for a 1D1V electrostatic plasma whose fast particles are speed-limited is derived and analyzed. By examining the normal modes of this dispersion relation, we show that the imposed speed-limiting substantially reduces the frequency of fast electron plasma oscillations while preserving the correct physics of lower-frequency plasma dynamics (e.g. ion acoustic wave dispersion and damping). We then demonstrate how the timestep constraints of conventional electrostatic particle-in-cell methods are relaxed by the speed-limiting approach, thus enabling larger timesteps and faster simulations. These results indicate that the SLPIC method is a fast, accurate, and powerful technique for modeling plasmas wherein electron kinetic behavior is nontrivial (such that a fluid/Boltzmann representation for electrons is inadequate) but evolution is on ion timescales.

This is the accepted manuscript version of the journal article whose reference is: T. G. Jenkins, G. R. Werner, and J. R. Cary, “Dispersion and the speed-limited particle-in-cell algorithm”, Phys. Plasmas **28**, 062107 (2021), <https://doi.org/10.1063/5.0046935>.

^{a)}tgjenkins@txcorp.com; <https://nucleus.txcorp.com/~tgjenkins>

I. INTRODUCTION

The speed-limited particle-in-cell (SLPIC) method¹ is a relatively new plasma modeling technique. It is most suitable for discharges in which the physics of interest occurs on relatively slow timescales (e.g., ion transport/profile relaxation) but is nevertheless tied to kinetic electron behaviors that a fluid/Boltzmann model cannot capture (e.g. distribution function modifications from neutral collisions or sheath interactions, or Landau damping). In such simulations, one is typically constrained to model both the heavy, slow ion species and the light, fast electrons using conventional particle-in-cell (PIC) techniques. The ensuing computational costs can be (possibly unaffordably) high; simulation timesteps must resolve the electron plasma frequency since kinetic electrons are present, but ion timescales of interest may exceed the electron oscillation period by many orders of magnitude.

In the SLPIC approach, conventional PIC is modified to artificially slow down ‘fast’ behaviors which are numerically troublesome, despite being physically unimportant for the physics of interest. Larger simulation timesteps can thus be used while retaining the detailed physics behaviors associated with the slower, longer timescales. The specifics of the SLPIC method will be explained in a later section of this paper, but we will note here that numerical experiments using SLPIC simulations to model sheath formation in an argon plasma have shown that remarkable speedup factors (160 times faster than conventional PIC methods²) can be achieved¹. When SLPIC can be appropriately used for modeling, it is both accurate and powerful.

A concept understood since the early days of PIC modeling is that while one may “recover more of the essence of the situation being simulated by changing the interaction laws”, such changes are accompanied by costs: “the more one meddles with the ‘laws’ of nature the more one must understand the consequences.”³ While this quote in its original context refers to the various approximations used in PIC simulation (e.g. finite-sized particles, grid spacings, and timesteps), in this paper we explore its relevance to SLPIC. Although SLPIC is in many ways similar to conventional PIC, the ways in which it is different introduce additional effects that one must understand in order to have confidence in its provided solutions – and this is true even independent of any effects imparted by finite-sized particles, grid spacings, and timesteps (though such effects are not unimportant). Fundamentally, SLPIC and PIC methods both seek to statistically approximate the evolution of smooth particle

distribution functions in a multidimensional phase space, in response to self-consistent fields and forces – but the underlying evolution equations of the two methods are different and will yield different physics (e.g. linear plasma wave dispersion) even before any particle-based approximations are made.

In this work, therefore, we focus on developing an understanding of the behavior of a plasma evolving with speed-limited dynamics (hereafter SLD). In SLD, the plasma is governed by continuous, ‘SLPIC-like’ equations of motion that differ from the ones governing plasma evolution in our universe, but which approximate them in certain limits that we will quantify. For purposes of comparison, we also designate the dynamics of plasma evolution in our universe as ‘ordinary dynamics’ (OD). SLPIC and PIC simulation methods are, respectively, the discrete numerical analogues of the SLD and OD that we will explore. [Alternatively, one can think of SLD or OD respectively as continuous limits of SLPIC or PIC, wherein both the timestep Δt and the grid spacing Δx approach zero as the velocity dependence of the distribution function f_α becomes smooth.] We will show that some well-understood physics processes from OD persist in SLD, and that other processes are substantially modified, some of them in very helpful ways.

More specifically, in this paper we derive and analyze the analytical dispersion relation in an electrostatic, collisionless, unmagnetized plasma evolving according to modified Vlasov-Poisson equations which govern SLD. Such a plasma will have different wave modes, with different dispersion, relative to a real plasma evolving with ordinary dynamics (OD). By comparison with the dispersive behavior that arises in the conventional (OD) Vlasov-Poisson system, we demonstrate both analytically and numerically that the speed-limiting of SLD can quantifiably modify high-frequency behaviors of this plasma (electron plasma oscillations) while leaving low-frequency motion (ion acoustic wave decay via electron Landau damping) undisturbed.

Section II of this paper explains the SLD concept, together with its connections both to the SLPIC algorithm and to the conventional kinetic theory of OD. In Section III, we discuss the behavior of an electrostatic ion-electron plasma that evolves with SLD, and derive the dispersion relation associated with this plasma. Section IV contains an analysis of the various waves permitted by this dispersion relation, together with the new behaviors imparted by SLD relative to known OD behaviors. We demonstrate that the speed-limiting significantly relaxes a fundamental numerical constraint associated with conventional PIC methods and

makes faster numerical simulation possible. Section V then considers the spatial fluctuation spectrum associated with SLD and shows it to be the same as that of OD; we briefly compare SLPIC and PIC simulations to demonstrate this point. Finally, in Section VI, we summarize our findings, review additional research directions which these findings might enable, and discuss various applications for the SLPIC concept in plasma modeling more generally.

II. PHASE SPACE EVOLUTION AND ITS CONNECTION TO PIC AND SLPIC METHODS

To kinetically model plasma with OD (i.e. using the familiar physics of the real world), we first consider the self-consistent evolution of a distribution function $\hat{f}_\alpha(\mathbf{x}, \mathbf{v}, t)$ of physical particles of species α . This distribution evolves according to a phase-space continuity equation

$$\frac{\partial}{\partial t} \hat{f}_\alpha(\mathbf{x}, \mathbf{v}, t) + \frac{\partial}{\partial \mathbf{x}} \cdot [\mathbf{v} \hat{f}_\alpha(\mathbf{x}, \mathbf{v}, t)] + \frac{\partial}{\partial \mathbf{v}} \cdot [\mathbf{a}(\mathbf{x}, \mathbf{v}, t) \hat{f}_\alpha(\mathbf{x}, \mathbf{v}, t)] = 0, \quad (1)$$

where $\mathbf{a}(\mathbf{x}, \mathbf{v}, t)$ is the self-consistent Lorentz acceleration experienced by a physical particle in the distribution at position \mathbf{x} with velocity \mathbf{v} at time t , in response to local (microscopic) electromagnetic fields. For Hamiltonian systems, the additional phase-space preserving constraint $(\partial/\partial \mathbf{x}) \cdot \mathbf{v} + (\partial/\partial \mathbf{v}) \cdot \mathbf{a} = 0$ of Liouville's theorem allows us to rewrite Eq. (1) in the familiar Klimontovich form

$$\frac{\partial}{\partial t} \hat{f}_\alpha(\mathbf{x}, \mathbf{v}, t) + \mathbf{v} \cdot \nabla \hat{f}_\alpha(\mathbf{x}, \mathbf{v}, t) + \mathbf{a} \cdot \frac{\partial}{\partial \mathbf{v}} \hat{f}_\alpha(\mathbf{x}, \mathbf{v}, t) = 0, \quad (2)$$

which can be formally solved by the method of characteristics. Along characteristic trajectories

$$\frac{d\mathbf{x}_{j\alpha}(t)}{dt} = \mathbf{v}_{j\alpha}(t), \quad (3)$$

$$\frac{d\mathbf{v}_{j\alpha}(t)}{dt} = \mathbf{a}[\mathbf{x}_{j\alpha}(t), \mathbf{v}_{j\alpha}(t), t], \quad (4)$$

the value of the distribution function $\hat{f}_\alpha[\mathbf{x}_{j\alpha}(t), \mathbf{v}_{j\alpha}(t), t]$ is preserved; writing the distribution function in the form

$$\hat{f}_\alpha(\mathbf{x}, \mathbf{v}, t) = \sum_{j=1}^{N_\alpha^p} \delta[\mathbf{x} - \mathbf{x}_{j\alpha}(t)] \delta[\mathbf{v} - \mathbf{v}_{j\alpha}(t)] \quad (5)$$

solves Eq. (2) and captures the detailed microscopic behavior of each of the N_α^p particles in response to the electromagnetic fields they (and the other species in the system) produce.

For realistic physical particle counts, this microscopic behavior is far too detailed to simulate numerically in most plasmas, and the singular nature of Eq. (5) is likewise problematic. If, instead, one passes to the continuum limit (subdividing the discrete particle charges and masses in a manner that preserves the local volumetric charge, mass, and energy content), one arrives at the Vlasov equation,

$$\frac{\partial}{\partial t} f_\alpha(\mathbf{x}, \mathbf{v}, t) + \mathbf{v} \cdot \nabla f_\alpha(\mathbf{x}, \mathbf{v}, t) + \mathbf{a} \cdot \frac{\partial}{\partial \mathbf{v}} f_\alpha(\mathbf{x}, \mathbf{v}, t) = 0, \quad (6)$$

which describes the evolution of a continuous (nonsingular) phase space fluid f_α from which the effects of particle discreteness have been removed. More detailed discussion of this transition, which considers ensemble averages of Eq. (2), two-particle and higher-order correlation terms, collision operators⁴, etc., has been considered by other authors⁵⁻⁷, but Eq. (6) suffices for our purposes here. Like Eq. (2), it can also be solved by the method of characteristics; with trajectories evolving according to Eqs. (3) – (4), we may formally write

$$f_\alpha(\mathbf{x}, \mathbf{v}, t) = \sum_{j=1}^{N_\alpha} w_{j\alpha}(t) \delta[\mathbf{x} - \mathbf{x}_{j\alpha}(t)] \delta[\mathbf{v} - \mathbf{v}_{j\alpha}(t)] \quad (7)$$

and can verify that it is a solution of Eq. (6). The smooth distribution is now represented as a set of N_α discrete macroparticles which evolve along the trajectories given by Eqs. (3 – 4). The weight function $w_{j\alpha}$ is representative (in some statistical sense) of the local value of f_α in a region near the particle's initial point on the phase space trajectory. PIC simulation techniques build upon the fundamental concept that Eqs. (3 - 4) and (7) solve Eq. (6), and that a sufficiently large number N_α of macroparticles, distributed so as to adequately resolve the relevant regions of the phase space, can statistically represent the 6D+time evolution of the smooth distribution function $f_\alpha(\mathbf{x}, \mathbf{v}, t)$.

In this paper we will consider Eqs. (3) - (4) and (6) as the fundamental equations describing plasma evolution under OD.

Techniques for mapping the equations of PIC onto discrete computational timesteps and finite grids (broadening the spatial extent of macroparticles from delta-functions to small-but-finite widths) are discussed extensively in existing literature^{3,8-13}; detailed explanations and/or derivations of such techniques will not be discussed here except as needed. For the

present it suffices to note (as the previously cited works discuss) that finite-sized grid cells and timesteps impose a number of constraints on conventional explicit PIC simulations:

- The *Debye length resolution constraint*, that a representative grid cell size Δx should adequately resolve the Debye length $\lambda_{D\alpha}$ associated with any of the species in the simulation in order to avoid numerical heating effects [the Debye length of species α is defined as $\lambda_{D\alpha}^2 \equiv \epsilon_0 T_\alpha / (q_\alpha^2 n_\alpha)$, where $\{q_\alpha, n_\alpha, T_\alpha\}$ are the species charge, density, and temperature (in units of energy) and ϵ_0 is the permittivity of free space];
- The *cell-crossing-time constraint*, that the distance traveled by any macroparticle in the simulation during a finite timestep Δt should not exceed a representative grid cell size Δx , so that forces experienced by a particle during a single simulation timestep are adequately resolved; and
- The *plasma oscillation constraint*, that the plasma frequency ω_p constrains the timestep through the relation $\omega_p \Delta t \leq 2$; otherwise, numerical instability of these high-frequency oscillations ensues [the plasma frequency is defined as $\omega_p^2 \equiv \sum_\alpha \omega_{p\alpha}^2$, with the species plasma frequency $\omega_{p\alpha}$ defined through $\omega_{p\alpha}^2 \equiv q_\alpha^2 n_\alpha / (\epsilon_0 m_\alpha)$. Here, m_α is the mass of species α and the other quantities were defined previously]. To be precise, this constraint arises from a more general requirement that every plasma mode frequency must be resolved by the simulation timestep. But for a large class of problems, including the ones considered in this work, the highest mode frequencies are on the order of ω_p .

These constraints can impose significant restrictions on a plasma simulation. Low temperatures and/or high densities decrease the Debye length and the allowable grid size, necessitating the use of finer grids and smaller timesteps. Further, when both cold, massive ions and hot, light electrons are simulated with PIC, the timesteps imposed by the plasma oscillation constraint (now dominated by fast electron motion since $\omega_p \sim \omega_{pe}$) are so small that ions may hardly move at all in that time interval. Numerical techniques such as subcycling¹⁵, in which ions are pushed less frequently and with a larger effective timestep, can provide minor computational savings, but this gains one at most a factor of ~ 2 in speedup (for typical cases with comparable electron and ion particle counts) since the timestep constraints

arising from electron motion remain. For simulations where many periods of harmonic ion motion are of interest, the number of timesteps required can be enormous.

The speed-limited particle-in-cell approach, and the more general speed-limiting concepts we explore in this work, are motivated by a desire to relax some of these constraints. The key idea is simple: the fastest particles and highest-frequency wave phenomena necessitate the smallest timesteps, and if these fast particle and wave motions can be slowed, the timestep constraints can be relaxed.

Accordingly, we introduce speed-limited dynamics (SLD), wherein equations from the derivation of the SLPIC method presented in Ref. 1 govern the plasma dynamics. Here, a distribution function f_α of species α evolves as prescribed by a modified Vlasov equation

$$\frac{\partial}{\partial t} f_\alpha(\mathbf{x}, \mathbf{v}, t) + \beta(\mathbf{v}) \mathbf{v} \cdot \frac{\partial}{\partial \mathbf{x}} f_\alpha(\mathbf{x}, \mathbf{v}, t) + \beta(\mathbf{v}) \mathbf{a} \cdot \frac{\partial}{\partial \mathbf{v}} f_\alpha(\mathbf{x}, \mathbf{v}, t) = 0, \quad (8)$$

wherein a speed-limiting function $\beta(\mathbf{v})$ in the range $(0, 1]$ has been introduced. This function transitions from values at or near unity (for “slow” particles) to values approaching $v_0/|\mathbf{v}|$ (for “fast” particles), and we can understand its effect by looking at the characteristic trajectories of the modified Vlasov equation

$$\frac{d\mathbf{x}(t)}{dt} = \beta[\mathbf{v}(t)] \mathbf{v}(t), \quad (9)$$

$$\frac{d\mathbf{v}(t)}{dt} = \beta[\mathbf{v}(t)] \mathbf{a}[\mathbf{x}(t), \mathbf{v}(t), t]. \quad (10)$$

The product $|\mathbf{v}|\beta(\mathbf{v})$, the speed at which an element of phase space changes its position $\mathbf{x}(t)$ as it moves through the phase space, now has value $\sim |\mathbf{v}|$ at low velocities but is limited to value v_0 (in the original vector direction of motion) at high velocities. We will hereafter refer to v_0 as the “speed limit”; it is the upper bound on the rate at which motion in the position coordinate of phase space may proceed. Accordingly, some nuance is required in discussing the phase space evolution since the meaning of ‘velocity’ is now ambiguous. An element of phase space has both a ‘true velocity’ (the phase space coordinate \mathbf{v}) and a ‘pseudo-velocity’ $d\mathbf{x}/dt = \beta\mathbf{v}$ (the speed and direction at which it is permitted to move from one physical space coordinate to another)¹⁴. In a given time interval, elements in the phase space with large true velocity $\mathbf{v}(t)$ [so that $\beta(\mathbf{v}) \ll 1$] experience both smaller pseudo-velocities [Eq. (9)] as they move through the space, and smaller changes to these pseudo-velocities (pseudo-acceleration) in response to applied forces [Eq. (10)]. Elements in the phase space with small true velocity experience no speed-limiting [$\beta(\mathbf{v}) \sim 1$] and evolve in the same

manner as their OD counterparts, as in Eqs. (3) and (4). Transitions across the boundary $|\mathbf{v}| = v_0$ in either direction are well-defined; this has already been demonstrated for SLPIC in Fig. 4 of Ref. 1, wherein particles are not observed to ‘pile up’ at the boundary.

In this paper we will consider Eqs. (8) - (10) as the fundamental equations describing plasma evolution under SLD.

Solutions to the SLD Vlasov equation, Eq. (8), can be represented statistically in the same manner as outlined above, setting

$$f_\alpha(\mathbf{x}, \mathbf{v}, t) = \sum_{j=1}^{N_\alpha} w_{j\alpha}(t) \delta[\mathbf{x} - \mathbf{x}_{j\alpha}(t)] \delta[\mathbf{v} - \mathbf{v}_{j\alpha}(t)] \quad (11)$$

for a suitably large number N_α of macroparticles evolving along the characteristic trajectories described by Eqs. (9) – (10). This is the speed-limited particle-in-cell method we have presented in previous work¹. However, this work will not focus on PIC or SLPIC implementations of Eqs. (6) or (8). Instead, we will consider these equations analytically.

III. A 1D1V ELECTROSTATIC PLASMA MODEL

In this section we will apply the Vlasov equation of OD and the modified Vlasov equation of SLD to model dispersion in an electrostatic, unmagnetized plasma with a single ion species, in one spatial dimension and one velocity-space dimension. We will use the analytic forms of these equations (foregoing for the moment any discussion of the effects of finite timesteps, grid spacings, or particle sizes) to ensure that we understand the new physics that the imposed speed-limiting of SLD imparts. Each species will use the kinetic equation

$$\frac{\partial f_\alpha(x, v, t)}{\partial t} + \beta(v)v \frac{\partial f_\alpha(x, v, t)}{\partial x} - \beta(v) \frac{q_\alpha}{m_\alpha} \frac{\partial \phi(x, t)}{\partial x} \frac{\partial f_\alpha(x, v, t)}{\partial v} = 0 . \quad (12)$$

In SLD, we will use a speed-limiting function of form

$$\beta(v) = -\frac{v_0}{v} + \left(\frac{v_0}{v} + 1\right) H(v + v_0) + \left(\frac{v_0}{v} - 1\right) H(v - v_0) , \quad (13)$$

wherein $H(x)$ is the Heaviside function. An equivalent representation for this speed-limiting function is

$$\beta(v) = \begin{cases} 1 & ; \quad |v| \leq v_0 \\ v_0/|v| & ; \quad |v| \geq v_0 \end{cases} . \quad (14)$$

In OD, $\beta(v) = 1$ (the $v_0 \rightarrow \infty$ limit of the SLD). The species couple via the Poisson equation,

$$\frac{\partial^2 \phi(x, t)}{\partial x^2} = - \sum_{\alpha} \frac{q_{\alpha}}{\epsilon_0} \int_{-\infty}^{\infty} f_{\alpha}(x, v, t) dv . \quad (15)$$

Many equilibrium solutions of Eq. (12) are possible. We will choose physically reasonable solutions that are stationary Maxwellians in each of the individual species (though we will allow the two species to have different temperatures, and neglect both the collisional processes that have brought the individual species to their present state and the interspecies collision processes that would further relax the system to a single temperature). Formally, we write the distribution function of species α as

$$f_{0\alpha}(x, v, t) = n_0 \sqrt{\frac{m_{\alpha}}{2\pi T_{0\alpha}}} \exp\left(-\frac{m_{\alpha} v^2}{2T_{0\alpha}}\right), \quad (16)$$

where n_0 is a species-independent constant number density, $T_{0\alpha}$ is the constant temperature of species α , and m_{α} is the species mass. With these equilibrium distributions, the corresponding equilibrium potential $\phi_0(x, t)$ is a constant that can be set to zero.

Linearizing Eqs. (12 – 13) in perturbed quantities, and Fourier transforming from space-time coordinates $\{x, t\}$ to wavenumber and frequency coordinates $\{k, \omega\}$, yields the result

$$-i\omega f_{\alpha 1}(k, v, \omega) + ik\beta(v)v f_{\alpha 1}(k, v, \omega) = \beta(v) \frac{q_{\alpha}}{m_e} ik\phi_1(k, \omega) \frac{\partial f_{\alpha 0}(v)}{\partial v}, \quad (17)$$

$$-k^2 \phi_1(k, \omega) = - \sum_{\alpha} \frac{q_{\alpha}}{\epsilon_0} \int_{-\infty}^{\infty} f_{\alpha 1}(k, v, \omega) dv . \quad (18)$$

We obtain, for the perturbed distribution functions,

$$f_{\alpha 1}(k, v, \omega) = \frac{kv\beta(v)}{\omega - kv\beta(v)} \frac{q_{\alpha}\phi_1(k, \omega)}{T_{0\alpha}} n_0 \sqrt{\frac{m_{\alpha}}{2\pi T_{0\alpha}}} \exp\left(-\frac{m_{\alpha} v^2}{2T_{0\alpha}}\right) \quad (19)$$

which we can then substitute into Eq. (18). The ensuing integrals will be undefined for resonant velocities $v\beta(v) = \omega/k$; we will implicitly stipulate that the integrals are to be evaluated using the Landau contour (traversing below any singularity) to retain both causality and the resonant physics. (Formally, this can be shown to be equivalent to the use of a Laplace transform, rather than a Fourier transform, in the time domain; it also permits the generalization of ω to complex values.) We obtain the integral relation

$$1 - \sum_{\alpha} \frac{q_{\alpha}^2 n_0}{k^2 \epsilon_0 T_{0\alpha}} \int_{-\infty}^{\infty} \frac{kv\beta(v)}{\omega - kv\beta(v)} \sqrt{\frac{m_{\alpha}}{2\pi T_{0\alpha}}} e^{-m_{\alpha} v^2 / (2T_{0\alpha})} dv = 0 \quad (20)$$

which describes the dispersive wave behavior of the plasma in both OD [where $\beta(v) = 1$] and SLD [where Eq. (14) defines $\beta(v)$].

In OD, the integral in Eq. (20) can be expressed in terms of the plasma dispersion function¹⁶, defined as

$$Z(\zeta) = \frac{1}{\sqrt{\pi}} \int_{-\infty}^{\infty} \frac{e^{-t^2}}{t - \zeta} dt \quad (21)$$

for $\text{Im}(\zeta) > 0$ and by its analytic continuation for $\text{Im}(\zeta) \leq 0$. In SLD, this integral is more complicated; given our choice for $\beta(v)$, there are both high-velocity regions of integration wherein $v\beta(v) = \pm v_0$, a constant (the speed limit), and low-velocity regions wherein $v\beta(v) = v$. We may represent the integrals over these various regions in terms of the complementary error function and the incomplete plasma dispersion function. The latter function was introduced by Franklin¹⁷ and its properties have been discussed extensively by Baalrud¹⁸; it takes the form [generalized from Eq. (21)]

$$Z(\gamma, \zeta) = \frac{1}{\sqrt{\pi}} \int_{\gamma}^{\infty} \frac{e^{-t^2}}{t - \zeta} dt \quad (22)$$

for $\text{Im}(\zeta) > 0$ and by its analytic continuation for $\text{Im}(\zeta) \leq 0$. It will be useful to note that $Z(-\infty, \zeta) = Z(\zeta)$ and that $Z(\infty, \zeta) = 0$. Additional properties of this function are provided in Appendix A.

In terms of these functions, we may rewrite Eq. (20) in the form $D_{SLD}(k, \omega; v_0) = 0$, where we define

$$D_{SLD}(k, \omega; v_0) \equiv 1 + \sum_{\alpha} \frac{1}{k^2 \lambda_{D\alpha}^2} \left[1 + \frac{\zeta_{\alpha}^2 \text{erfc}(\gamma_{\alpha})}{\gamma_{\alpha}^2 - \zeta_{\alpha}^2} + \zeta_{\alpha} [Z(-\gamma_{\alpha}, \zeta_{\alpha}) - Z(\gamma_{\alpha}, \zeta_{\alpha})] \right]. \quad (23)$$

Here, we make use of the parameters $\gamma_{\alpha} \equiv v_0/(\sqrt{2}v_{t\alpha})$, a measure of the relative speed-limiting of species α ; $\zeta_{\alpha} = \omega/(\sqrt{2}kv_{t\alpha})$, the conventional (and complex) argument of the plasma dispersion function; $\lambda_{D\alpha}^2 \equiv \epsilon_0 T_{0\alpha}/(q_i^2 n_0)$, the Debye length of species α ; and $v_{t\alpha}^2 \equiv T_{0\alpha}/m_{\alpha}$, the thermal velocity for species α . The complementary error function is related to the conventional error function by $\text{erfc}(x) \equiv 1 - \text{erf}(x)$. The expression $D_{SLD}(k, \omega; v_0) = 0$ is the plasma dispersion relation of SLD, and its analysis and solutions will be the topic of the following section.

Recalling that $\text{erfc}(\infty) = 0$ and the limits of the incomplete plasma dispersion function discussed above, we can show that $D_{SLD}(k, \omega; \infty) = D_{OD}(k, \omega)$, where the latter function

has the explicit form

$$D_{OD}(k, \omega) = 1 + \sum_{\alpha} \frac{1}{k^2 \lambda_{D\alpha}^2} [1 + \zeta_{\alpha} Z(\zeta_{\alpha})], \quad (24)$$

a standard result from elementary plasma kinetic theory^{19,20}. This is the plasma dispersion relation of OD, against which solutions with SLD will be compared.

IV. ANALYSIS OF THE DISPERSION RELATION

We now consider various limits of $D_{OD}(k, \omega)$ and $D_{SLD}(k, \omega; v_0)$, together with the waves that arise in these various limits. For clarity, we will consider the physics of OD first, and will then explore the changes which the speed-limiting of SLD imparts to these familiar processes.

A. Plasma oscillations

The OD dispersion relation, Eq. (24), admits approximate analytic solutions corresponding to cold-plasma oscillations in the $\zeta_{\alpha} \gg 1$ limit. The asymptotic expansion of $Z(\zeta_{\alpha})$ in this limit,

$$Z(\zeta_{\alpha}) \sim -\frac{1}{\zeta_{\alpha}} \left(1 + \frac{1}{2\zeta_{\alpha}^2} + \frac{3}{4\zeta_{\alpha}^4} + \dots \right) + \mathcal{O}(e^{-\zeta_{\alpha}^2}) \quad (25)$$

can be substituted into Eq. (24) to obtain, at lowest order,

$$D_{OD}(k, \omega) = 1 - \frac{\omega_{pe}^2}{\omega^2} - \frac{\omega_{pi}^2}{\omega^2} = 0 \quad (26)$$

where $\omega_{p\alpha}^2 = q_i^2 n_0 / (\epsilon_0 m_{\alpha})$ is the square of the plasma frequency of species α . These oscillations are dominated by electron motion (the ion term is order m_e/m_i smaller than the electron term); we may write the solution as $\omega^2 = \omega_{pe}^2 (1 + m_e/m_i) \equiv \omega_p^2$. We anticipate the prospect of significant changes to these oscillations in SLD, since the speed-limiting will preferentially modify the fast electron motion.

What is the behavior of the SLD dispersion relation, Eq. (23), in the same $\zeta_{\alpha} \gg 1$ limit? Using the asymptotic expansions for $Z(\gamma, \zeta)$ presented in Ref. 18 and summarized in Appendix A, we can show that the SLD version of Eq. (26) takes the form

$$D_{SLD}(k, \omega; v_0) = 1 - \sum_{\alpha} \frac{\omega_{p\alpha}^2}{\omega^2} \left(1 + (2\gamma_{\alpha}^2 - 1) \text{erfc}(\gamma_{\alpha}) - \frac{2\gamma_{\alpha} e^{-\gamma_{\alpha}^2}}{\sqrt{\pi}} \right) = 0 \quad (27)$$

which reproduces Eq. (26) in the $v_0 \rightarrow \infty$ (i.e. $\gamma_\alpha \rightarrow \infty$) limit. It admits the solutions

$$\omega^2 = \sum_{\alpha} \omega_{p\alpha}^2 h(\gamma_\alpha) \quad ; \quad h(\gamma_\alpha) \equiv \left(1 + (2\gamma_\alpha^2 - 1)\text{erfc}(\gamma_\alpha) - \frac{2\gamma_\alpha e^{-\gamma_\alpha^2}}{\sqrt{\pi}} \right). \quad (28)$$

The behavior of the function $h(\gamma_\alpha)$ is shown in Figure 1. For small γ_α , $h(\gamma_\alpha) \sim 2\gamma_\alpha^2$, while for large γ_α , the species is not appreciably speed-limited and $h(\gamma_\alpha) \approx 1$. Recalling that $\gamma_\alpha = v_0/\sqrt{2}v_{t\alpha}$, it will be instructive to express the argument of h strictly in terms of the electron slowing-down parameter γ_e ; we have $\gamma_i = \gamma_e \sqrt{T_e m_i / (T_i m_e)}$. The presence of the ion-electron mass ratio suggests that unless electrons are much cooler than ions, the quantity γ_i will always be much larger than γ_e . Accordingly, we may generally choose v_0 in a way that alters electron behavior but not ion behavior, consistent with the intentional slowing down of the fastest particles in SLD while leaving slower particles undisturbed. Such a v_0 will be faster than most ions but much slower than most electrons. For such a choice ($v_0 = 4v_{ti}$), Figure 1 also shows values of γ_e, γ_i , and their corresponding h values for a hydrogen plasma thermalized to 10 eV. In this plasma, ion motion associated with plasma oscillations does not differ appreciably between SLD and OD, but electron motion is considerably modified.

Since it is primarily the speed-limiting of electrons that affects the oscillation frequencies predicted by Eq. (28), we examine the behavior of these modified electron plasma oscillations as a function of the ratio v_0/v_{te} (providing intuition as to which velocities in a typical electron distribution, e.g. a Maxwellian, are restricted by the speed-limiting). The normalized oscillation frequency of Eq. (28) is shown in Fig. (2) for a monatomic hydrogen plasma with equal electron and ion temperatures. While the oscillation frequencies of SLD and OD are identical at large values of v_0/v_{te} (minimal speed-limiting), reducing this ratio, and hence increasing the corresponding fraction $\text{erfc}(\gamma_e)$ of speed-limited electrons, reduces the SLD frequency monotonically. As $v_0/v_{te} \rightarrow 0$, the linear approximation to the plasma frequency approaches the heuristic estimate made in Ref. 1: $\omega/\omega_p \sim v_0/v_{te}$. The high-frequency oscillations of OD have been mapped to lower-frequency oscillations in SLD by the speed-limiting of electrons.

We conclude that in SLD, the frequency of conventional electron-dominated plasma oscillations is reduced relative to OD. In Sec. IV C we will consider how this reduction relaxes the ‘plasma oscillation constraint’ referred to in Sec. II. But we must first determine whether the speed-limited dynamics preserves physics associated with lower-frequency waves.

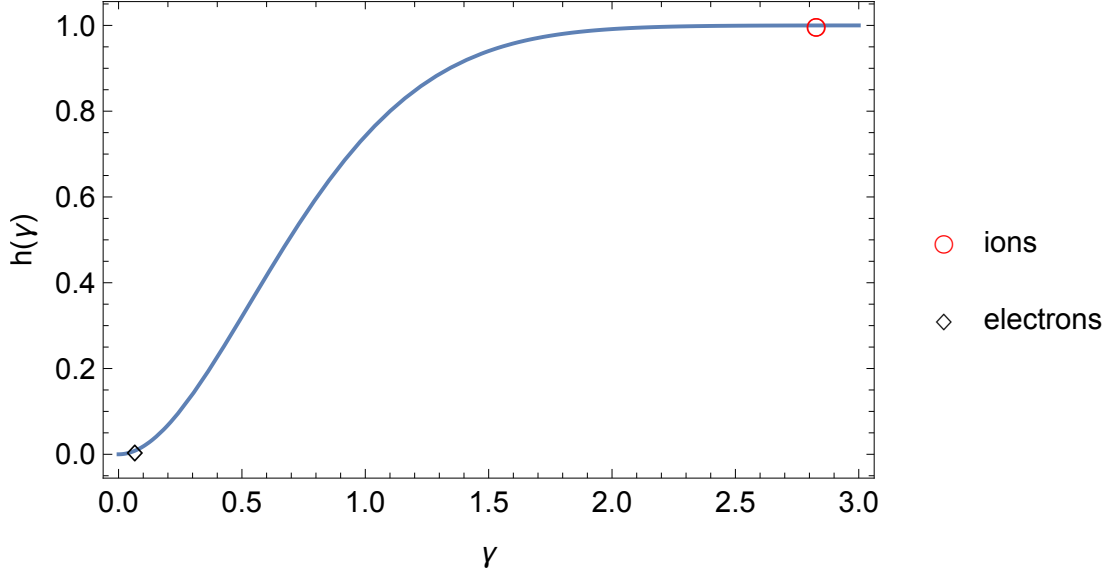


FIG. 1. Behavior of the function $h(\gamma_\alpha)$ in Eq. (28) as a function of the species speed-limiting parameter $\gamma_\alpha = v_0/(\sqrt{2}v_{t\alpha})$. For high values of v_0 relative to the species thermal velocity, speed-limiting does not occur in densely populated portions of the phase space and this function (a multiplicative factor in the dispersion relation) approaches unity. When $v_{ti} \ll v_0 \ll v_{te}$, considerable speed-limiting of the electron distribution can be achieved without appreciable effect on the ion distribution, such that $h(\gamma_e) \ll 1$ while $h(\gamma_i) \approx 1$. To illustrate this point, values of γ_α and the ensuing $h(\gamma_\alpha)$ are shown for a case with $v_0 = 4v_{ti}$, in a hydrogen plasma with both species at temperature 10 eV.

B. Ion acoustic waves

The OD dispersion relation, Eq. (24), also admits approximate analytic solutions corresponding to ion acoustic waves. Physically, these solutions are associated with ‘hot’ electrons ($\zeta_e \ll 1$) and ‘cold’ ions ($\zeta_i \gg 1$), and in these limits the dispersion relation can be written in the approximate form

$$k^2\lambda_{De}^2 D_{OD}(k, \omega) = 1 + k^2\lambda_{De}^2 + \zeta_e i\sqrt{\pi} - \frac{k^2 c_s^2}{\omega^2} = 0, \quad (29)$$

where the multiplicative factor of $k^2\lambda_{De}^2$ simplifies the algebra and where c_s , the sound speed, satisfies the relation $c_s^2 = T_{0e}/m_i$. Assuming that the imaginary part of the (now complex)

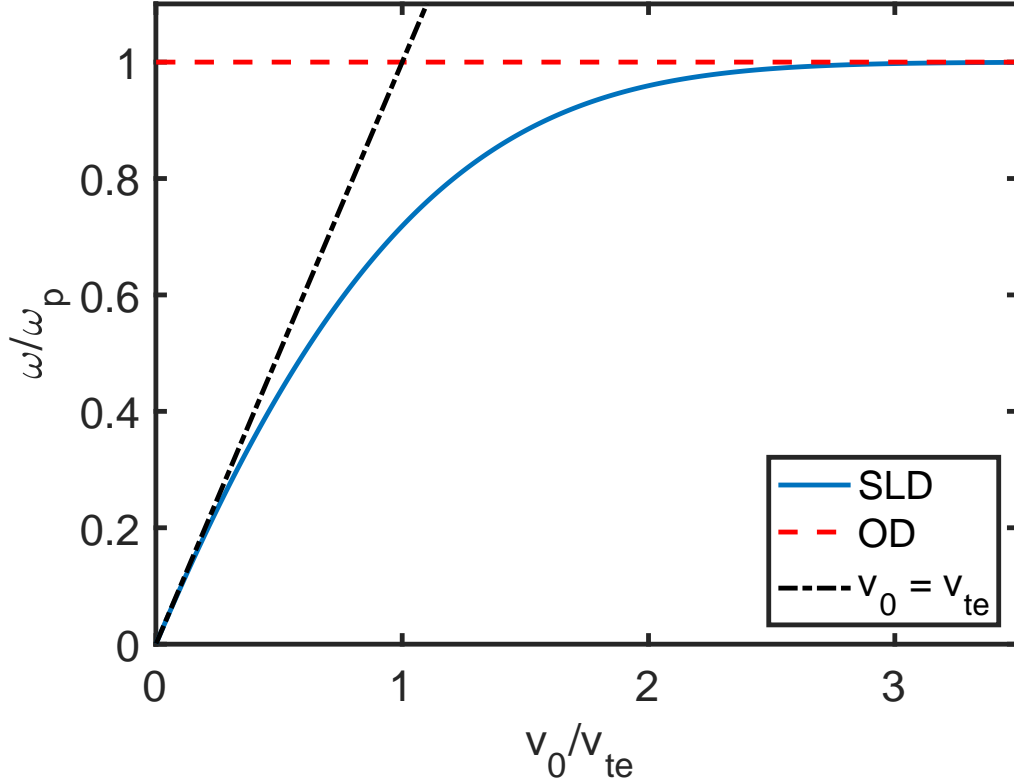


FIG. 2. Frequency of electron-dominated cold plasma oscillations in SLD and OD as a function of the ratio of speed limit to electron thermal speed ($v_0/v_{te} = \sqrt{2}\gamma_e$). The electron-dominated cold plasma oscillation frequency is constant in OD (red dashed line), but in SLD it unphysically decreases (blue solid line) as v_0/v_{te} is reduced. This unphysical frequency means that plasma oscillations are not correctly simulated, but this can greatly speed up simulation when plasma oscillations are unimportant to the physics of interest. When $v_0 \ll v_{te}$, $\omega/\omega_p \sim v_0/v_{te}$.

$\omega = \omega_r + i\omega_i$ is small, we can perform a Taylor expansion,

$$D(k, \omega) \approx D(k, \omega_r) + i\omega_i \left. \frac{\partial D(k, \omega)}{\partial \omega} \right|_{\omega=\omega_r} \quad (30)$$

to show that this equation permits damped wavelike solutions of the form

$$\omega = \pm \frac{kc_s}{\sqrt{1 + k^2\lambda_{De}^2}} - i\sqrt{\frac{\epsilon\pi}{8}} \frac{kc_s}{(1 + k^2\lambda_{De}^2)^2} \quad (31)$$

where ϵ is again the electron/ion mass ratio. These are the ion acoustic wave (IAW) modes, which are essentially longitudinal compressions of the ion mass density that decay via Landau damping.

What is the corresponding behavior of the SLD dispersion relation? In the $\zeta_i \gg 1, \zeta_e \ll 1$ limit, Eq. (23) can be written with the same multiplicative factor in the form

$$k^2 \lambda_{De}^2 D_{SLD}(k, \omega; v_0) = 1 + k^2 \lambda_{De}^2 - \frac{k^2 c_s^2}{\omega^2} h(\gamma_i) + i\sqrt{\pi} \zeta_e [H(\zeta_e - \gamma_e) - H(\zeta_e + \gamma_e)] = 0. \quad (32)$$

Repeating the Taylor expansion procedure above, we can show that the ion acoustic wave dispersion relation of SLD has approximate analytic solutions

$$\omega = \pm \omega_r - i \sqrt{\frac{\epsilon \pi}{8}} \frac{k c_s h(\gamma_i)}{(1 + k^2 \lambda_{De}^2)^2} \left[H\left(\frac{\omega_r}{k} + v_0\right) - H\left(\frac{\omega_r}{k} - v_0\right) \right], \quad (33)$$

wherein

$$\omega_r \equiv \frac{k c_s \sqrt{h(\gamma_i)}}{\sqrt{1 + k^2 \lambda_{De}^2}}. \quad (34)$$

This is the SLD equivalent to Eq. (31). The OD and SLD forms are approximately equivalent provided that γ_i is sufficiently large (so that $h(\gamma_i) \sim 1$, see Fig. 1) and $|\omega_r/k| < v_0$ (so that the speed limit v_0 exceeds the phase velocity of the ion acoustic wave). Since the approximation $h(\gamma_i) \approx 1$ holds to one part in 10^4 or better for $v_0 > 4v_{ti}$, we will write these constraints as a single condition

$$v_0 > \max(4v_{ti}, |\omega_r/k|). \quad (35)$$

When v_0 is chosen to satisfy this condition, and when the other conditions we assumed in the derivation [$\zeta_i \gg 1, \zeta_e \ll 1, \text{Im}(\omega) \ll \text{Re}(\omega)$] are valid, the effects of SLD on the propagation and damping of the IAW are minimal.

What happens when the phase velocity condition is violated, such that $v_0 < |\omega_r/k|$? In this case, the explicitly imaginary terms in Eq. (32) (proportional to Heaviside functions) vanish, and the solutions admitted now only capture the real part of Eq. (33). While the IAW still propagates, its Landau damping is not correctly modeled. This is consistent with a result that we have demonstrated in previous work¹, namely, that the correct dynamics of resonant wave-particle interactions cannot be captured by speed-limited particle-in-cell simulations when particles whose velocities were previously synchronous with the wave velocity are speed-limited. Particles whose speed-limiting renders them unable to keep up with the wave

cannot exchange energy with it, so the dissipative effects which lead to wave damping are effectively turned off. Although nothing in principle prevents us from choosing a smaller v_0 value that violates Eq. (35), the inherent advantage of the velocity-dependent speed-limiting approach (preservation of IAW physics) would be lost in doing so.

The analytic form of the IAW above is approximate. The dispersion relation can also be solved numerically to find the complex ω associated with a given k , and we have done so for a plasma with density $n_0 = 5.0 \times 10^{16} \text{ m}^{-3}$, $T_{e0} = 10 \text{ eV}$, and $T_{i0} = 1/40 \text{ eV}$. In the supplemental materials for Ref. 18, Matlab algorithms for evaluating $Z(\zeta)$, $Z(\gamma, \zeta)$, and their derivatives have been provided. We have made use of these algorithms and Matlab minimization routines to compute $\{\omega, k\}$ values which satisfy the OD and SLD dispersion relations within a given tolerance, according to norm-minimization criteria

$$\sqrt{|D_{SLD}(k, \omega; v_0)|^2} \leq \delta_{SLD} , \quad (36)$$

$$\sqrt{|D_{OD}(k, \omega)|^2} \leq \delta_{OD} . \quad (37)$$

Here, the tolerance parameter $\delta \ll 1$ is a small positive number which constrains the allowable error in the numerical solution of a particular dispersion relation. In these computations we fix k (and, for SLD, v_0), and then numerically evaluate the function D for various complex values of ω . Exact solutions to the dispersion relation have $D = 0$; we vary ω in the complex plane in a manner that seeks to minimize the norm of D and thus to approach these exact solutions. For ω values near an exact solution this norm can in principle be reduced to be no greater than δ .

Various values for the speed-limiting parameter v_0 can be chosen to assess the effect of speed-limiting on IAW behavior. Depending on the value of v_0 and k , to obtain numerical convergence it is sometimes necessary to raise δ_{SLD} to values as high as 10^{-3} , but solutions can usually be found for $\delta_{OD} < 10^{-6}$ and $\delta_{SLD} < 10^{-5}$ (and often for δ values that are several orders of magnitude smaller, when $k \gg 1$).

In Fig. 3, we show the real and negative-imaginary parts of the computed frequency ω for various values of wavenumber k spanning several orders of magnitude. In this figure, the speed limit v_0 has the value $0.2v_{te}$; the analytic approximation to the dispersion relation (valid for $k\lambda_{De} \lesssim 1$) is also shown. The speed-limiting does not affect the IAW behavior appreciably; for modes whose wavelengths are large compared to the Debye length (i.e. where the analytic approximation is valid) the SLD real frequency ω is about half a percent

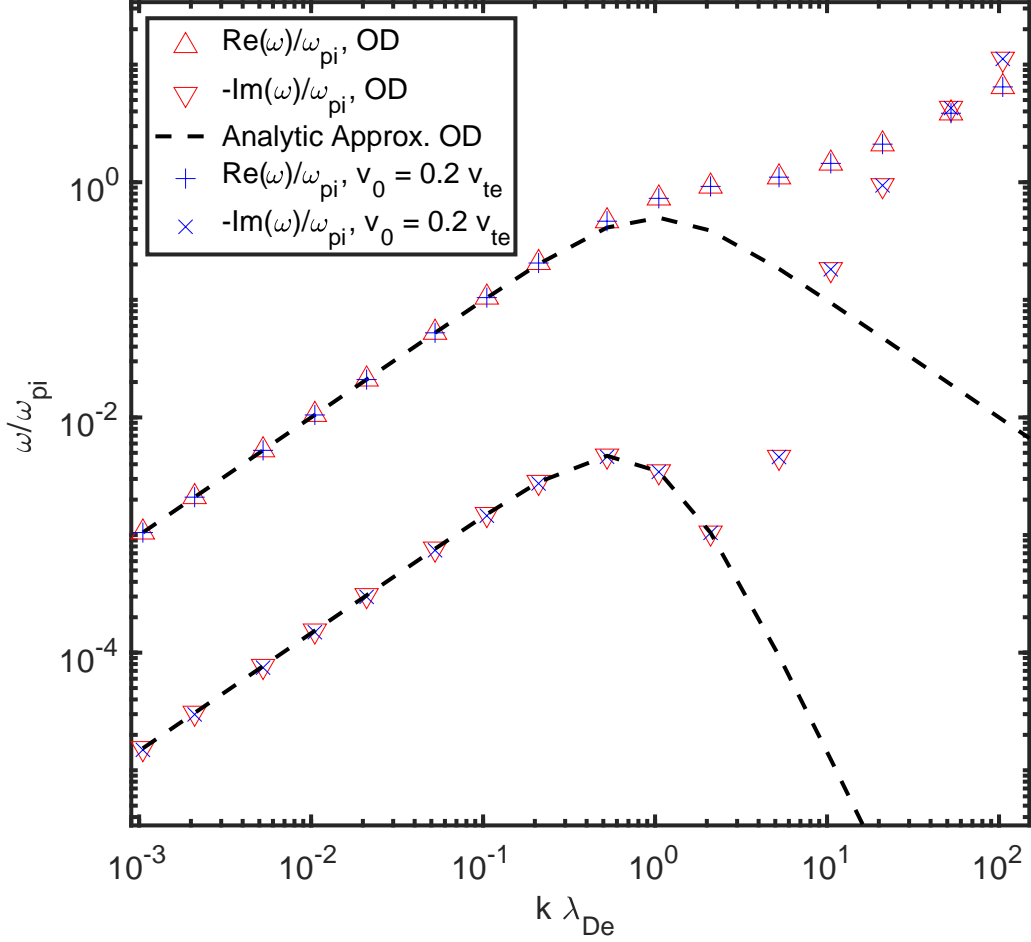


FIG. 3. Real and negative-imaginary parts of the normalized IAW frequency, computed numerically from the OD (red) and SLD (blue) dispersion relations, as a function of normalized wavenumber. Values from the approximate analytic expression, Eq. (31), are also shown (dashed black curves) and agree well with the exact solutions when $k\lambda_{De} \lesssim 1$. In the SLD case the speed limit $v_0 = 0.2v_{te}$. Even though all electrons are restricted to move through the domain with speeds no greater than v_0 , the frequency (good to within 0.5%) and damping rate (good to within 3%) for the ion acoustic wave do not differ appreciably from the OD values. Good agreement between SLD and OD is maintained even in the $k\lambda_{De} > 1$ regime, where the analytic approximations underlying Eq. (31) are no longer valid.

low relative to the OD value and the SLD damping rate also drops by about 3%. For shorter-wavelength modes, the effect of the speed-limiting on both the real frequencies and damping rates is negligible. Nevertheless, the frequency of the modified plasma oscillations [from Fig. (2)] is decreased to about $0.2\omega_{pe}$ for this case.

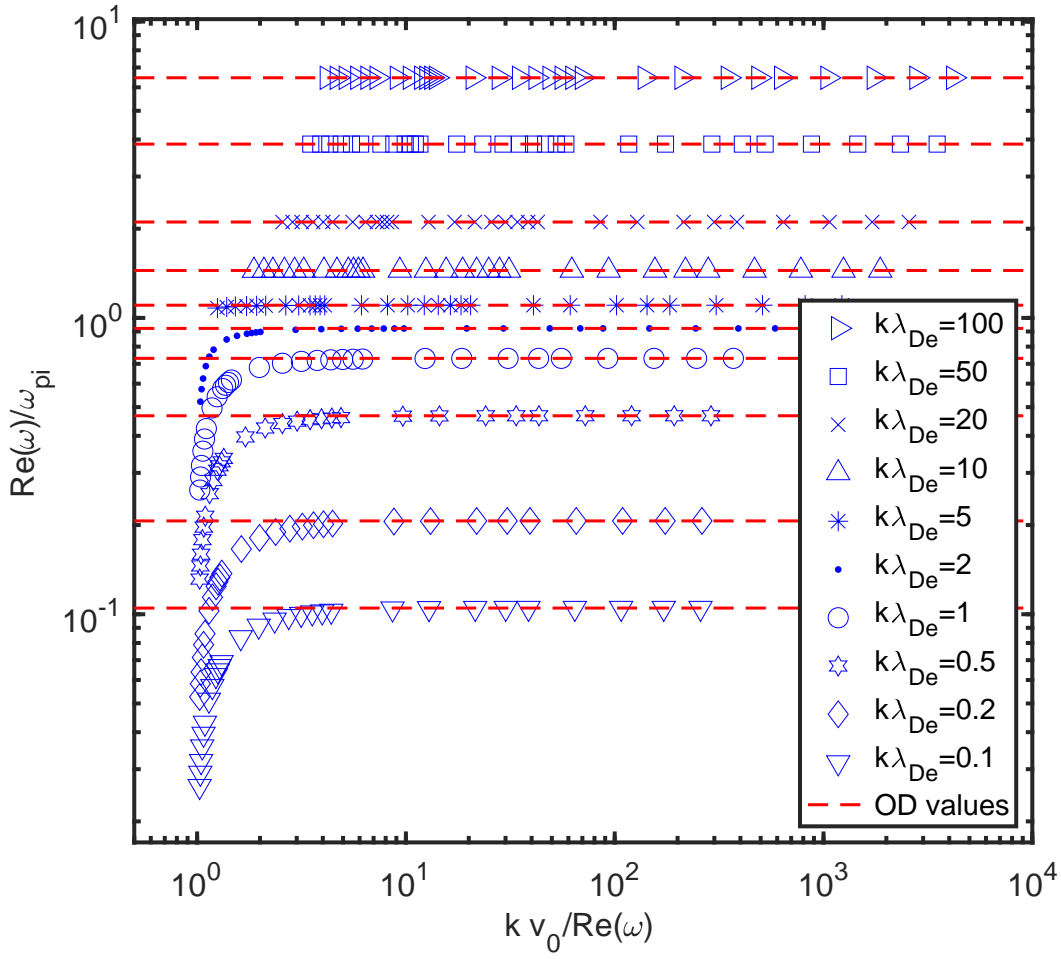


FIG. 4. Variation of the normalized real part of the frequencies which solve the ion acoustic branch of the SLD dispersion relation, as a function of the speed limit v_0 normalized to the wave phase velocity $v_\phi = \text{Re}(\omega)/k$, for various values of $k\lambda_{De}$. The OD frequencies, which are independent of v_0 , are also shown for each $k\lambda_{De}$ value (red dashed lines). Although speed-limiting does not affect the mode frequencies for $v_0/v_\phi \gg 1$, modes whose wavelengths are large compared to the Debye length ($k\lambda_{De} \lesssim 1.0$) are reduced in frequency as the speed limit is reduced (moving to the left on the graph) to be of the same order as the phase velocity. This frequency variation is minimal for $v_0 > 5v_\phi$ and also for modes whose wavelengths are short relative to the Debye length. For this case $v_{ti}/v_{te} = 0.05\sqrt{m_e/m_i}$.

For more restrictive speed limits v_0 , greater deviation of IAW frequencies and damping rates from their non-speed limited (OD) values is observed, though still only for modes whose wavelengths are long compared to the Debye length. Generally speaking, real frequencies are shifted downward as the speed limit is decreased, though only by a few percent (<9%

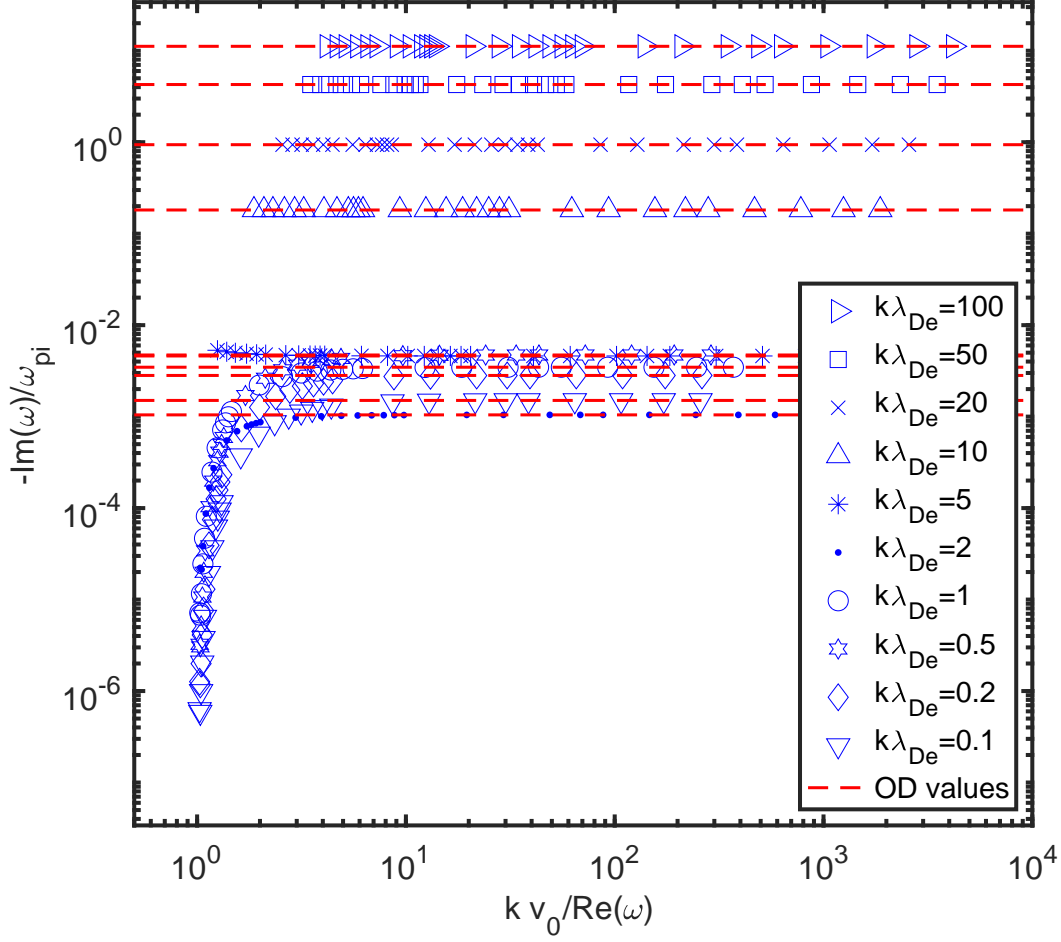


FIG. 5. Variation of the normalized negative-imaginary part (damping rate) of the frequencies which solve the ion acoustic branch of the SLD dispersion relation, as a function of the speed-limit v_0 normalized to the wave phase velocity $v_\phi = \text{Re}(\omega)/k$, for various values of $k\lambda_{De}$. The OD damping rates, which are independent of v_0 , are also shown for each $k\lambda_{De}$ value (red dashed lines). Although speed-limiting does not affect the damping rates when $v_0/v_\phi \gg 1$, damping rates for modes whose wavelengths are large compared to the Debye length ($k\lambda_{De} \lesssim 1.0$) may be reduced by several orders of magnitude as the speed limit is reduced (moving to the left on the graph) to be of the same order as the phase velocity. As is also true for the real frequencies (Fig. 4), the damping rate variation is minimal for $v_0 > 5v_\phi$ and also for modes whose wavelengths are short relative to the Debye length. For this case $v_{ti}/v_{te} = 0.05\sqrt{m_e/m_i}$.

for $v_0 = 0.05v_{te} = 2.1c_s$, and $<2\%$ for $v_0 = 0.1v_{te} = 4.2c_s$). Damping rates also (generally) decrease in magnitude as the speed limit is decreased, but the magnitude of the relative decrease is larger ($<42\%$ for $v_0 = 0.05v_{te} = 2.1c_s$, $<13\%$ for $v_0 = 0.1v_{te} = 4.2c_s$). In Figures

4 and 5 we have plotted the variation of the IAW real frequency and damping rate of SLD as a function of the speed-limiting velocity normalized to the wave phase velocity, so as to more generally quantify the effect of the speed-limiting on the IAW dispersive behavior. These figures illustrate that lowering the speed limit has relatively little effect on either the real IAW oscillation frequency or damping rate as long as the speed limit is higher than the wave phase velocity. For longer-wavelength modes ($k\lambda_{De} \lesssim 1$) in SLD, speed limits that approach the wave phase velocity generally give rise to modest reductions in the mode frequency (Fig. 4) and more pronounced reductions of the IAW damping rate (Fig. 5). This failure to properly capture the Landau damping of the IAW arises because portions of the distribution function that resonate with the wave (in OD) are prevented from doing so by the imposed speed-limiting¹. As we transition to shorter-wavelength modes (moving up the graph legend), absolute damping rates are increased to become comparable to the real mode frequency, while phase velocities are reduced to be of order v_{ti} . For these waves, speed-limiting does not appreciably influence the dynamics since the smallest sensible speed limit ($v_0 \sim 4v_{ti}$, so as not to speed-limit the bulk ion distribution) still exceeds $v_\phi = \omega/k$ for large k .

Accordingly, we may assert that SLD preserves the physics of IAW propagation and damping provided that the condition in Eq. (35) holds, namely, when ions are not speed-limited and when the speed limit reasonably exceeds the phase velocity of the IAWs in the system. At the same time, this speed limiting considerably reduces the frequency of plasma oscillations (as was shown in Section IV A).

C. Normal modes and the plasma oscillation constraint

Having explored the normal modes of our 1D1V plasma, we now revisit the numerical constraints which the use of a finite timestep Δt will impose on particle-in-cell simulations of this plasma.

We have noted in Section II that numerical instability will ensue in a PIC simulation if the frequency of any plasma mode is not resolved, and that in particular, we must resolve the frequency associated with electron plasma oscillations. These oscillations are generally the highest-frequency modes in a PIC simulation containing electrons (because ions introduce only small corrections to the approximation $\omega_p \approx \omega_{pe}$ when the electron-ion mass ratio is

small). Accordingly, any numerical simulation method satisfying the constraint $\omega_p \Delta t \geq 2$ will resolve both these plasma oscillations and all other modes of lower frequency.

What is the effect of the speed limiting on this constraint?

Because of the speed-limiting, the frequency that we must resolve is now not ω_p ; rather, it is the fastest oscillation frequency that the speed-limiting permits. But we have shown in Sec. IV that ordinarily ‘fast’ plasma oscillations [see Eq. (28)] are considerably slowed in SLD. Thus, in its most general form, SLPIC replaces the plasma oscillation constraint by the result [obtained by substituting the frequency derived in Eq. (28) for ω_p]

$$\Delta t \leq \frac{2}{\sqrt{\omega_{pe}^2 h(\gamma_e) + \omega_{pi}^2 h(\gamma_i)}} \approx \frac{2}{\omega_{pe} \sqrt{h(\gamma_e)}} \quad (38)$$

where $\gamma_\alpha = v_0/\sqrt{2}v_{t\alpha}$ is the slowing-down parameter. [For example, when $v_0/v_{te} = 0.1$, we have $\gamma_e = 0.07$, $h(\gamma_e) \approx 9.5 \times 10^{-3}$, and $1/\sqrt{h(\gamma_e)} \approx 10$, thus relaxing the constraint tenfold with minimal effect on the ion modes (assuming IAW phase velocities are low compared to v_0).] This constraint is less restrictive than the PIC result $\Delta t \leq 2/\omega_{pe}$, and permits larger timesteps to be taken in SLPIC simulations without instability or loss of accuracy in the low-frequency plasma modes. It can also be shown that by limiting the maximum speed to v_0 , SLPIC trivially relaxes the cell-crossing-time constraint by nearly the same factor (see Appendix B). Both the plasma oscillation constraint and the cell-crossing-time constraint are thus modified by speed-limiting to restrict $\Delta t \sim \Delta x/v_0$.

V. ANALYSIS OF THE FLUCTUATION SPECTRUM

From the fluctuation-dissipation theorem and the theory of linear response, the fluctuation spectrum of an electrostatic 1D plasma in thermal equilibrium can be shown¹³ to take the form

$$\frac{\epsilon_0 \langle E^2 \rangle(k)}{T_0} = \frac{1}{D(k, \omega = \infty)} - \frac{1}{D(k, \omega = 0)}, \quad (39)$$

where T_0 is the equilibrium temperature, $\langle E^2 \rangle(k)$ is the time-average of the continuous spatial Fourier transform of the square of the electric field, and $D(k, \omega)$ is the dispersion relation. In OD, taking these limits of Eq. (24) yields the result

$$\left(\frac{\epsilon_0 \langle E^2 \rangle(k)}{T_0} \right)_{OD} = \frac{1}{1} - \frac{1}{1 + \sum_\alpha \frac{1}{k^2 \lambda_{D\alpha}^2}} = \frac{1}{1 + k^2 \lambda_D^2}, \quad (40)$$

wherein $\lambda_D^2 \equiv \epsilon_0 T_0 / \sum_\alpha (q_\alpha^2 n_\alpha)$ is the square of the plasma Debye length.

What is the behavior of the SLD fluctuation spectrum? At low frequencies, where speed-limiting is not expected to influence the wave dynamics, we likewise recover the same result as for OD:

$$D_{SLD}(k, \omega = 0; v_0) = 1 + \sum_\alpha \frac{1}{k^2 \lambda_{D\alpha}^2} . \quad (41)$$

At high frequencies, we have shown that the behavior of solutions to the dispersion relation is significantly altered by the speed-limiting. Nevertheless, terms associated with speed-limiting vanish in the high-frequency limit of the dispersion relation

$$D_{SLD}(k, \omega = \infty; v_0) = 1 + \sum_\alpha \frac{1}{k^2 \lambda_{D\alpha}^2} \left(1 - \operatorname{erfc}(\gamma_\alpha) - \frac{\operatorname{erfc}(-\gamma_\alpha)}{2} + \frac{\operatorname{erfc}(\gamma_\alpha)}{2} \right) = 1 \quad (42)$$

[because $\operatorname{erfc}(-x) \equiv 2 - \operatorname{erfc}(x)$]; the effects of speed-limiting should therefore have no bearing on the spatial fluctuation spectrum, Eq. (39). We recover the same result as Eq. (40) for SLD,

$$\left(\frac{\epsilon_0 \langle E^2 \rangle(k)}{T_0} \right)_{SLD} = \frac{1}{1 + k^2 \lambda_D^2} . \quad (43)$$

In a PIC or SLPIC simulation, the fluctuation spectra of Eqs. (40) and (43) are altered by finite particle size (associated with the transfer of charge and force fields between continuous particle positions and the discrete grid) as well as by finite grid spacing (associated with the wavenumber spectrum that is able to be resolved by the simulation). In addition, the introduction of a discrete grid and a finite volume leads to discrete, finite Fourier spectra and introduces the possibility of aliasing between gridded fields and subgrid particle modes. While we do not propose to discuss the effects of finite particle and grid size in detail in this work, we have used PIC and SLPIC to simulate a 1D single-ion-species hydrogen plasma in thermal equilibrium and have measured its fluctuation spectrum. For a discrete Fourier mode this spectrum satisfies a relation of the general form^{10,12,13}

$$\frac{\epsilon_0 |E_l|^2}{n_0 T_0} = \frac{1}{N_p} \left(\frac{1}{1 + K^2 \lambda_D^2 / |S(k)|^2} \right) \quad (44)$$

wherein N_p is the number of simulation macroparticles of either species, $|S(k)|^2$ is a geometric factor associated with the particle shape, $k = 2\pi l/L$ defines the discrete mode index l , $K = k \operatorname{sinc}(k\Delta/2)$ captures the effect of the 1D Laplacian operator on the discrete 1D grid with spacing Δ [with $\operatorname{sinc}(x) \equiv \sin(x)/x$], and $|E_l|^2$ is the time-averaged norm of the l -th discrete mode in the Fourier transform of the electric field.

We modeled this scenario with the VSim²¹ code, using both PIC with a small timestep ($\Delta t = 1.0 \times 10^{-13}$ s) and SLPIC with a (50X) larger timestep. We used a highly resolved grid (80 cells per Debye length, with a 1D simulation length $L = 10$ Debye lengths), with equilibrium plasma density $n_0 = 5.0 \times 10^{16} \text{ m}^{-3}$ and temperature $T_0 = 10$ eV. 100 particles per cell of each species were used; the speed limit v_0 for the SLPIC simulations was set to one-half the electron thermal velocity. Particles were mapped to the grid with a three-cell (four-gridpoint) stencil using the method prescribed by Esirkepov²². For this mapping, $|S(k)|^2 = \text{sinc}^8(k\Delta/2)$. As shown in Figure 6, both PIC and SLPIC capture the general behavior of the fluctuation spectrum when the effects of finite grid size and particle width are accounted for. Larger variation between adjacent modes in the spectrum is observed for SLPIC relative to PIC, an effect which becomes more prominent as γ_e is decreased (stronger speed-limiting) and which is perhaps a function of interparticle correlations imposed by the speed-limiting constraint (since all fast particles now move with the same pseudo-velocity in the domain). Nevertheless, both methods agree closely with the theory. SLPIC simulations with smaller timesteps (identical to PIC) were not seen to differ substantially from the large-timestep result (green curve) in the figure.

A more detailed consideration of the role of finite grid spacing and particle width in SLPIC is a topic of ongoing interest, and we anticipate future efforts along these lines.

VI. CONCLUSIONS

In this paper we have discussed the linear wave dispersion in a 1D1V unmagnetized electrostatic plasma that evolves with both ordinary (OD) and speed-limited (SLD) dynamics. We have demonstrated that speed-limiting can effectively reduce the frequency of fast electron oscillations while quantitatively preserving low-frequency ion and electron motion, e.g. the physics needed to correctly model the Landau damping of ion acoustic waves. We have also shown that this speed-limiting relaxes the “plasma oscillation constraint” of the conventional PIC method, permitting larger timesteps, and have demonstrated that the spatial dependence of the ensuing fluctuation spectrum is nevertheless preserved. These findings suggest that the speed-limited particle-in-cell (SLPIC) method, as outlined in previous work¹, is a fast, accurate, and powerful technique for modeling plasmas wherein electron kinetic behavior is significant (such that a fluid/Boltzmann representation for electrons is in-

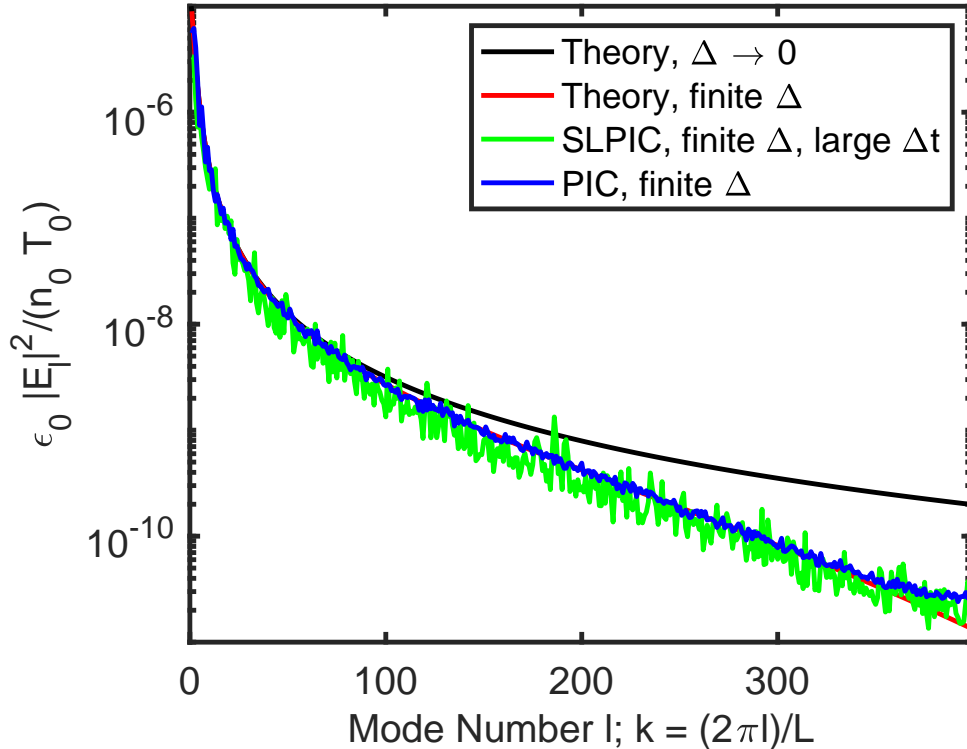


FIG. 6. Predicted fluctuation spectrum in the limit of infinite grid resolution and zero particle size (black), together with the predicted behavior for finite grid resolution and particle shape (red – and covered by the PIC data except at very high mode numbers), and the observed spectra from SLPIC (green) and PIC (blue) simulations. While the signals vary more with k for SLPIC than for PIC, both methods agree closely with the theory for finite Δ .

adequate) but evolution is on ion timescales. In these cases the use of PIC is computationally demanding, but the use of speed-limited electrons can substantially reduce computational demands without sacrificing the desired physics.

For plasmas with $v_{ti} \ll v_\phi \ll v_{te}$ [where these velocities respectively are the ion thermal velocity, ion acoustic wave phase velocity ω/k ($\sim c_s$ for long-wavelength modes), and the electron thermal velocity], the speed limit v_0 can be chosen with $v_\phi < v_0 < v_{te}$. Choosing $v_0 < v_{te}$ ensures that the speed-limited plasma oscillation frequency is reduced below the true plasma oscillation frequency ω_p by a factor $\omega/\omega_p \sim v_0/v_{te}$, and allows the timestep to

be increased (and the simulation sped up) by a factor v_{te}/v_0 . However, choosing $v_0 > v_\phi$ ensures that ion acoustic waves are still accurately simulated (including the Landau damping rate).

Potential applications for the SLPIC method include its use in the modeling of plasma thrusters (wherein very small electron/ion mass ratios impose especially demanding numerical constraints) and sheath formation (e.g. near a Langmuir probe²³). Collisional low-temperature plasma discharges are also an area of particular interest; recent efforts have demonstrated that SLPIC can be used in conjunction with standard Monte Carlo collision techniques, in the same manner as is done in collisional PIC discharge modeling (PIC-MCC)²⁴. We anticipate exploring SLPIC's capability for rapid collisional plasma discharge modeling in future publications.

ACKNOWLEDGMENTS

This research was financially supported by the U.S. Department of Energy, SBIR Phase I/II Award DE-SC0015762, and by the U.S. National Science Foundation, Grant PHY1707430. The data that support the findings of this work are available from the corresponding author upon reasonable request. We thank the reviewers of this manuscript for their constructive comments.

Appendix A: Asymptotic expansions of $Z(\gamma, \zeta)$

A detailed overview of the properties of the incomplete plasma dispersion function $Z(\gamma, \zeta)$ was given by Baalrud in Ref. 18. A number of these relations have been used in this work and are summarized here.

For $\zeta \gg 1$:

$$Z(\gamma, \zeta) \sim i\sigma\sqrt{\pi}H(\zeta - \gamma)e^{-\zeta^2} - \frac{\text{erfc}(\gamma)}{2\zeta} - \frac{e^{-\gamma^2}}{2\sqrt{\pi}\zeta^2} - \frac{1}{\zeta^3} \left(\frac{\gamma e^{-\gamma^2}}{2\sqrt{\pi}} + \frac{\text{erfc}(\gamma)}{4} \right) - \dots \quad (\text{A1})$$

wherein $H(x)$ is the Heaviside function, $\text{erfc}(x)$ is the complementary error function $\text{erfc}(x) = 1 - \text{erf}(x)$, and

$$\sigma = 1 - \text{sign}[\text{Im}(\zeta)] . \quad (\text{A2})$$

For $\zeta \ll 1$:

$$Z(\gamma, \zeta) \sim i\sqrt{\pi}H(\zeta - \gamma)e^{-\zeta^2} + \frac{E_1(\gamma^2)}{2\sqrt{\pi}} + \zeta \left(\frac{e^{-\gamma^2}}{\gamma\sqrt{\pi}} - \operatorname{erfc}(\gamma) \right) + \zeta^2 \left(\frac{e^{-\gamma^2}}{2\sqrt{\pi}\gamma^2} - \frac{E_1(\gamma^2)}{2\sqrt{\pi}} \right) + \dots \quad (\text{A3})$$

wherein

$$E_1(x) = \int_1^\infty \frac{e^{-xt}}{t} dt \quad (\text{A4})$$

is the exponential integral.

Matlab algorithms for evaluating $Z(\zeta)$, $Z(\gamma, \zeta)$, and their derivatives were also provided in the supplemental materials for Ref. 18. These algorithms were used in the numerical calculations of this work.

Appendix B: Constraints and speed-limiting

In this appendix we briefly consider the scaling of the numerical constraints outlined in Section II in SLD.

The Debye length resolution constraint is independent of the speed-limiting. When it is satisfied, the grid size $\Delta x = \delta\lambda_{De}$ for some $\delta \lesssim 1$.

In SLD, the cell-crossing time constraint is altered by the speed-limiting and becomes $v_0\Delta t < \Delta x$, since no particle can move faster than the speed limit v_0 . Substituting the result from the Debye length resolution constraint then yields the scaling $\Delta t < \delta\lambda_{De}/v_0$.

The plasma oscillation constraint, in the limit of aggressive speed-limiting ($\gamma_e \rightarrow 0$), replaces $\omega_p \sim \omega_{pe}$ by $\omega_{pe}v_0/v_{te}$ (as shown in the small- γ limit of Fig. 1). Substituting the result from the Debye length resolution constraint then yields the scaling $\Delta t < 2v_{te}/(v_0\omega_{pe}) = 2\lambda_{De}/v_0$.

It is significant that the timestep Δt restriction scales linearly as the ratio of Debye length to speed limit in both of the latter two constraints. If this were not so, there could be regions of parameter space where one constraint or the other prevailed, and the speed-limiting concept would be less useful. But the physical scaling for both constraints is the same – the largest timestep for speed-limited particles is on the order of the time required for the fastest such particles to cross a Debye length. This restriction preserves the physics of local Debye shielding (a time-independent phenomena) even while slowing the rapid plasma oscillations. In addition, this constraint is independent of the electron-ion mass ratio, suggesting that

SLPIC can be used even when this ratio is small.

Appendix C: Comparison of speed-limited and relativistic dynamics

It has been noted that SLD exhibits some similarities with relativistic dynamics, wherein the speed of light c plays a role somewhat analogous to the SLD speed limit v_0 . Although we haven't explored this idea in detail in this work, it is instructive to compare the kinetic equation for nonrelativistic SLD [using a more general Lorentz acceleration term that includes the electromagnetic fields $\mathbf{E}(\mathbf{x}, t)$ and $\mathbf{B}(\mathbf{x}, t)$] with the relativistic kinetic (Vlasov) equation in the form

$$\frac{\partial f_\alpha}{\partial t} + \beta \mathbf{v} \cdot \frac{\partial f_\alpha}{\partial \mathbf{x}} + \beta \frac{q_\alpha}{m_\alpha} \mathbf{E} \cdot \frac{\partial f_\alpha}{\partial \mathbf{v}} + \beta \frac{q_\alpha}{m_\alpha} \mathbf{v} \times \mathbf{B} \cdot \frac{\partial f_\alpha}{\partial \mathbf{v}} = 0 \quad (\text{SLD}) \quad (\text{C1})$$

$$\frac{\partial g_\alpha}{\partial t} + \frac{1}{\gamma} \mathbf{u} \cdot \frac{\partial g_\alpha}{\partial \mathbf{x}} + \frac{q_\alpha}{m_\alpha} \mathbf{E} \cdot \frac{\partial g_\alpha}{\partial \mathbf{u}} + \frac{1}{\gamma} \frac{q_\alpha}{m_\alpha} \mathbf{u} \times \mathbf{B} \cdot \frac{\partial g_\alpha}{\partial \mathbf{u}} = 0 \quad (\text{relativistic}) . \quad (\text{C2})$$

Here, respectively, the SLD distribution $f_\alpha = f_\alpha(\mathbf{x}, \mathbf{v}, t)$ is a function of position, velocity, and time, while the relativistic distribution $g_\alpha = g_\alpha(\mathbf{x}, \mathbf{p}, t)$ is a function of position, momentum, and time. The spatial components of the four-velocity, $\mathbf{u} \equiv (\mathbf{p}/m_\alpha)$, are related to the conventional three-velocity \mathbf{v} through the relativistic Lorentz factor $\gamma = \sqrt{1 + \mathbf{u} \cdot \mathbf{u}/c^2}$, such that $\mathbf{u} = \gamma \mathbf{v}$.

The structure of these equations is very similar. The relativistic \mathbf{u} (whose magnitude may exceed c) is like the SLD ‘true velocity’ \mathbf{v} (whose magnitude may exceed v_0), and the factor $1/\gamma$ (~ 1 for $|\mathbf{u}| \ll c$, and $\sim c/|\mathbf{u}|$ for $|\mathbf{u}| \gg c$) plays a role akin to the speed-limiting function β (~ 1 for $|\mathbf{v}| \ll v_0$, and $\sim v_0/|\mathbf{v}|$ for $|\mathbf{v}| \gg v_0$). The product of these relativistic functions, \mathbf{u}/γ (three-velocity), can never exceed c just as the SLD ‘pseudo-velocity’ can never exceed v_0 .

Nevertheless, key differences appear. The term proportional to the electric field, in the relativistic case, contains no physics equivalent to the speed-limiting that occurs in SLD – in effect, relativistic physics applies the speed-limiting concept to the magnetic, but not the electric, components of the Lorentz acceleration. The ensuing trajectories thus vary from those of SLPIC, wherein the appearance of β in all but the first term of Eq. (C1) can be viewed as a local rescaling of time (with β) along a trajectory that is constant regardless of the value of v_0 . So while SLD is somewhat like relativistic dynamics, in that it tracks both unbounded (SLD true velocity/relativistic momentum) and bounded (SLD pseudo-

velocity/relativistic three-velocity) phase space variables, with the latter restricted by fixed speed limits (SLD v_0 /relativistic c), the dynamics of the two systems differ enough to make intuitive comparisons difficult.

REFERENCES

- ¹G. R. Werner, T. G. Jenkins, A. M. Chap, and J. R. Cary, *Phys. Plasmas* **25**, 123512 (2018).
- ²Subsequent code development has enabled speedup factors of greater than 250 for this discharge, relative to conventional PIC. Detailed discharge properties are provided in Ref. 1.
- ³A. B. Langdon and C. K. Birdsall, *Phys. Fluids* **13**, 2115 (1970).
- ⁴Collisional effects, which would replace the zero on the right-hand side of Eq. (1) with source or sink terms, could also be included in this equation; SLPIC is compatible with conventional PIC-MCC techniques for modeling collisional plasmas. We will not consider collisional effects in this work, but future publications demonstrating collisional SLPIC discharges are anticipated.
- ⁵D. C. Montgomery, *Theory of the Unmagnetized Plasma*, Gordon and Breach, 1971.
- ⁶D. G. Swanson, *Plasma Kinetic Theory*, CRC Press, 2008.
- ⁷B. Scheiner and P. J. Adrian, *Phys. Plasmas* **26**, 034501 (2019).
- ⁸C. K. Birdsall and A. B. Langdon, *Plasma Physics via Computer Simulation*, CRC Press, 2004.
- ⁹R. W. Hockney and J. W. Eastwood, *Computer Simulation Using Particles*, CRC Press, 1988.
- ¹⁰A. B. Langdon, *J. Comp. Phys.* **6**, 247 (1970).
- ¹¹H. Okuda and C. K. Birdsall, *Phys. Fluids* **13**, 2123 (1970).
- ¹²H. Okuda, *Phys. Fluids* **15**, 1268 (1972).
- ¹³A. B. Langdon, *Phys. Fluids* **22**, 163 (1979).
- ¹⁴Parallels can be drawn with relativistic dynamics, in which elements of phase space can move from one physical position to another with speed no faster than the speed of light; see Appendix C for further discussion.
- ¹⁵J. C. Adam, A. Gourdin Serveniére, and A. B. Langdon, *J. Comp. Phys.* **47**(2), 229 (1982).

- ¹⁶B. D. Fried and S. D. Conte, *The Plasma Dispersion Function*, Academic Press, 1961.
- ¹⁷R. N. Franklin, in *Proceedings of the Tenth International Conference on Phenomena in Ionized Gases*, page 269, Donald Parsons and Company, Ltd., 1971.
- ¹⁸S. D. Baalrud, *Phys. Plasmas* **20**, 012118 (2013).
- ¹⁹R. J. Goldston and P. H. Rutherford, *Introduction To Plasma Physics*, IoP, 1995.
- ²⁰F. F. Chen, *Introduction to Plasma Physics and Controlled Fusion*, Springer, 3rd edition, 2016.
- ²¹C. Nieter and J. R. Cary, *J. Comp. Phys.* **196**, 448 (2004).
- ²²T. Zh. Esirkpov, *Comp. Phys. Comm.* **135**(2), 144 (2001).
- ²³G. R. Werner, S. Robertson, T. G. Jenkins, A. M. Chap, and J. R. Cary, “Accelerated Steady-State Electrostatic Particle-in-Cell Simulation of Langmuir Probes”, to be submitted to *Phys. Plasmas*.
- ²⁴J. Theis, G. R. Werner, T. G. Jenkins, and J. R. Cary, *Phys. Plasmas* **28**, 063513 (2021).